Spin alignment of stars in old open clusters

Enrico Corsaro[1,2,3,4], Yueh-Ning Lee[1], Rafael A. García[1], Patrick Hennebelle[1], Savita Mathur[5], Paul G. Beck[1], Stephane Mathis[1], Dennis Stello[6,7] & Jérôme Bouvier[8]

Stellar clusters form by gravitational collapse of turbulent molecular clouds, with up to several thousand stars per cluster[1]. They are thought to be the birthplace of most stars and therefore play an important role in our understanding of star formation, a fundamental problem in astrophysics[2,3]. The initial conditions of the molecular cloud establish its dynamical history until the stellar cluster is born. However, the evolution of the cloud's angular momentum during cluster formation is not well understood[4]. Current observations have suggested that turbulence scrambles the angular momentum of the cluster-forming cloud, preventing spin alignment amongst stars within a cluster[5]. Here we use asteroseismology[6–8] to measure the inclination angles of spin axes in 48 stars from the two old open clusters NGC 6791 and NGC 6819. The stars within each cluster show strong alignment. Three-dimensional hydrodynamical simulations of proto-cluster formation show that at least 50% of the initial proto-cluster kinetic energy has to be rotational in order to obtain strong stellar-spin alignment within a cluster. Our result indicates that the global angular momentum of the cluster-forming clouds was efficiently transferred to each star and that its imprint has survived after several gigayears since the clusters formed.

About half of the overall star formation in the Milky Way is occurring in the 24 most massive giant molecular clouds[1]. The star forming regions are obscured by dust, hence direct observations are limited to the infrared and radio bands[2,3]. However, open clusters can be studied in a broad range of wavelengths because they contain small amounts of interstellar gas and dust. The great advantage of studying stars in a cluster — as opposed to field stars that often originate from dissolved small stellar systems — is that they can preserve the signature of the initial conditions of the progenitor molecular cloud.

It is believed that molecular clouds satisfying the Jeans instability undergo gravitational fragmentation in which the internal motions are strongly influenced by turbulence[4,9]. This suggests that the angular momentum from the progenitor cloud cannot leave any significant imprint of its action on the stars born in the cluster. However, if the stars inherit the physical properties of the molecular cloud, they should to some extent reflect its average angular momentum. To investigate the angular momentum imprint, requires measurements of the space orientation of the stellar-spin axis. Previous analyses conducted on young open clusters did not find evidence of stellar-spin alignment[5].

Asteroseismology, the study of stellar oscillations, has proven to be a powerful tool to obtain model-independent information on the inclination angle of the stellar angular momentum vector,

[1]Laboratoire AIM Paris-Saclay, CEA/DRF — CNRS — Université Paris Diderot, IRFU/SAp Centre de Saclay, F-91191 Gif-sur-Yvette Cedex, France [2]Instituto de Astrofísica de Canarias, E-38200 La Laguna, Tenerife, Spain [3]Departamento de Astrofísica, Universidad de La Laguna, E-38205 La Laguna, Tenerife, Spain [4]INAF - Osservatorio Astrofisico di Catania, Via S. Sofia 78, I-95123 Catania, Italy [5]Space Science Institute, 4750 Walnut street Suite 205, Boulder, CO 80301, USA [6]Sydney Institute for Astronomy (SIfA), School of Physics, University of Sydney, Sydney, New South Wales 2006, Australia [7]Stellar Astrophysics Centre, Department of Physics and Astronomy, Aarhus University, Ny Munkegade 120, DK-8000 Aarhus C, Denmark [8]Université Grenoble Alpes, IPAG, F-38000 Grenoble, France; CNRS, IPAG, F-38000 Grenoble, France

especially for red giant stars[7,8,10,11]. Red giants are typically low- and intermediate-mass stars that have evolved off the main sequence of the stellar evolution. Most red giants oscillate and their oscillations can be analyzed through a Fourier frequency spectrum of their light curve. The spectrum of a red giant contains a comb-like structure of tens and sometimes more than a hundred radial and non-radial oscillation modes, most of which are mixed modes originating by the coupling between acoustic and gravity modes[12]. Each oscillation mode is identified by an angular degree l, which gives rise to a multiplet of $(2l + 1)$ different components through the degeneracy lifted by the stellar rotation[6]. Each rotationally split component is in turn identified by an azimuthal number, $m \leq |l|$. The dipolar ($l = 1$) mixed modes are the most suited for measuring the orientation of the spin axis in red giants[13].

We have investigated 48 oscillating red giant stars, with typical masses within the range ~ 1.1-$1.7\,M_{\odot}$ ($M_{\odot}$ being the mass of the Sun), that belong to the open clusters NGC 6791 and NGC 6819[14–16]. The most relevant physical properties of the two open clusters are outlined in Table 1. Both clusters are old, with NGC 6791 being one of the oldest known in our Galaxy[17], which implies that the initial molecular clouds were massive enough to ensure that the cluster evaporation time — the time it takes for all the members of a cluster to be ejected by internal stellar encounters — is well beyond the gigayear (Gyr) time scale. We used four years of time-series photometry obtained by NASA's Kepler mission. We measure the asteroseismic properties[18,19] of a total of about 380 rotationally split dipolar mixed modes — identified from a set of more than 3900 oscillation modes — and we use them to measure the spin-inclination angles (see Methods and Supplementary Fig. 1 for an example of the fits to the oscillation modes).

The distributions of the spin inclinations (Fig. 1), show that about 70% of the stars in each cluster have a strong level of alignment, with a low to mid angle for NGC 6791 ($\theta \approx 30^{\circ}$ and an alignment coefficient $\alpha \simeq 0.77$) and a low angle for NGC 6819 ($\theta \approx 20^{\circ}$, $\alpha \simeq 0.74$), close to a pole-on configuration (see Methods for more details, and Supplementary Tables 1 and 2 for a list of all the results). We also notice a clear cut-off for higher angles (mid to high) in both clusters, where instead a larger number of stars would be expected if the spin vectors were uniformly (randomly) distributed in three dimensions. The binary stars identified in NGC 6819 appear to follow a similar alignment trend to that of the single star members of the cluster. The probability that the observed levels of alignment are the result of a random distribution is less than 1 in 10^9 for NGC 6791, and 1 in 10^7 for NGC 6819. Conversely, the distribution obtained for an independent sample of 36 field red giants (not members of any cluster) shows no significant stellar-spin alignment ($\alpha \simeq 0.38$), even when considering subsamples of stars in the same evolutionary stage ($\alpha \simeq 0.41$ for shell-H-burning and $\alpha \simeq 0.35$ for core-He-burning stars, respectively, see Methods and Supplementary Table 5). In addition our reanalysis of an independent sample of main-sequence stars in NGC 6819 hinting at high spin-inclination angles from their rotational periods and projected equatorial velocities[20], reveals that their period measurements are not reliable and hence not in conflict with our low-inclination results (see Methods and Supplementary Fig. 2 and 3 for more details). In Fig. 2 we provide the spatial positions of the cluster red giants within fields of view approximately corresponding to the observed size of each cluster, as reported in Table 1. The stars appear to sample the entire field of each cluster, with a tangential distance from star to star varying from ≈ 0.1 parsec (pc) near the center up to a few pc in the peripheral regions. This demonstrates that the spin alignment is observed across the entire clusters.

N-body simulations coupled with observations of old open clusters, aimed at reproducing their dynamical evolution, show that the stellar angular momentum can have an impact on colliding stars and on the orbital configurations of multiple stellar systems[21]. The orbital parameters of eccentricity, inclinations, and periods of multiple stellar systems are mostly influenced by tidal forces[22]. For individual stars the angular momentum typically evolves as a spin down over time[20] through either

mass loss by stellar winds, magnetic braking, or tidal friction if the star is captured to form a binary. Given the average distances among the star members of an open cluster, the effect of gravitational N-body interactions on producing any significant spin alignment is negligible even for timescales of several Gyr. This is especially true for tidal forces, because their strength is a function of the inverse third power of the distance between two stars. Furthermore, using the galactic latitudes and distance moduli reported in Table 1, the heights of the two clusters from the galactic plane are $\approx 800\,$pc and $\approx 350\,$pc for NGC 6791 and NGC 6819, respectively, showing that they are located far from the most crowded regions that constitute the inner galactic disk. The position and long survival time of the two clusters therefore suggests that they experienced significantly less disruptive encounters with giant molecular clouds than other open clusters located inside the disk[23]. This means that the strong spin alignment observed in the red giants of our sample is very likely to be originating from the formation epoch of the cluster, thus preserving the signature of the early dynamical processes characterizing the progenitor molecular cloud.

For exploring this scenario we have performed three-dimensional hydrodynamical simulations of a collapsing molecular cloud leading to the formation of a proto-cluster under the action of gravitational potential[24] (see Methods for further explanations). Figure 3a shows that when considering only a turbulent velocity field, the distribution of the resulting spin inclinations resembles that of a uniform orientation in three dimensions. By introducing a global rotation as an additional initial condition and imposing a ratio of rotational kinetic energy over turbulent kinetic energy of $E_{\rm rot}/E_{\rm tur} \simeq 1$, the spin alignment produced in stars forming with masses greater than $0.7\,M_{\odot}$ becomes comparable to that found in our observations, with $\alpha \simeq 0.6$ (Fig. 3b and c). When $E_{\rm rot}/E_{\rm tur} < 1$ instead, the spin alignment is only marginal (see Supplementary Table 3 for all the values we investigated). From our simulations we also observe that for stellar masses below $0.7\,M_{\odot}$ the turbulent motions still dominate over the effect of rotation even in the case $E_{\rm rot}/E_{\rm tur} \simeq 1$, thus preventing any spin alignment among stars of this low mass range. This suggests that when not enough mass from the molecular cloud is accreted into individual pre-stellar cores, the information from the cloud's average angular momentum is lost in the stellar-spin fluctuations induced by turbulence at the scales of the forming star. A strong component of the cloud's rotational kinetic energy, at least comparable to that of the turbulence, can therefore be responsible of efficiently aligning the spin axes within the stellar members of a cluster because the degree of alignment reflects the importance of the cloud's average angular momentum. The two open clusters NGC 6791 and NGC 6819 could have originated through a formation process involving a compact collapsing molecular cloud giving rise to a rotating proto-cluster (Fig. 3c). During the cluster formation, stars with masses at least that of our Sun are more likely to inherit a significant fraction of the cloud's average angular momentum with respect to stars having masses below $0.7\,M_{\odot}$. By measuring stellar spin inclinations for solar-mass stars in open clusters we can therefore constrain the initial energy budget of the progenitor molecular cloud, its global rotation, as well as the efficiency by which the cloud's average angular momentum is transferred to the individual stellar members of the clusters. This result allows us to explore and reconstruct the dynamical evolution, structure, and geometry of galactic star forming regions that have formed stellar clusters back in times comparable to the age of our Universe.

1. Lee, E. J., Murray, N., Rahman, M. Milky Way Star-forming Complexes and the Turbulent Motion of the Galaxy's Molecular Gas. *Astrophys. J.* **752**, 146-159 (2012).
2. Longmore, S. N., *et al.* Protostars and Planets VI (eds. H. Beuther, R. Klessen, C. Dullemond, Th. Henning) Ch. 13. Univ. of Arizona Press, (291, 2014).
3. Lada, C. J. & Lada, E. A. Embedded Clusters in Molecular Clouds. *Ann. Rev. Astron. & Astrophys.* **41**, 57-115 (2003).
4. McKee, C. F. & Ostriker, E. C. Theory of Star Formation. *Ann. Rev. Astron. & Astrophys.* **45**, 565–687 (2007).

5. Jackson, R. J. & Jeffries, R. D. Are the spin axes of stars randomly aligned within a cluster? *Mon. Not. R. Astron. Soc.* **402**, 1380-1390 (2010).
6. Gizon, L. & Solanki, S. K. Determining the Inclination of the Rotation Axis of a Sun-like Star. *Astrophys. J.* **589**, 1009-1019 (2003).
7. Beck, P. G. *et al.* Fast core rotation in red-giant stars as revealed by gravity-dominated mixed modes. *Nature* **481**, 55–57 (2012).
8. Huber, D. *et al.* Stellar Spin-Orbit Misalignment in a Multiplanet System. *Science* **342**, 331(2013).
9. Urquhart, J. S. *et al.* ATLASGAL - towards a complete sample of massive star forming clumps. *Mon. Not. R. Astron. Soc.* **443**, 1555–1586 (2014).
10. Ballot, J., García, R. A., Lambert, P. Rotation speed and stellar axis inclination from p modes: how CoRoT would see other suns. *Mon. Not. R. Astron. Soc.* **369**, 1281–1286 (2006).
11. Benomar, O. *et al.* Nearly uniform internal rotation of solar-like main-sequence stars revealed by space-based asteroseismology and spectroscopic measurements. *Mon. Not. R. Astron. Soc.* **452**, 2654–2674 (2015).
12. Bedding, T. R. *et al.* Gravity modes as a way to distinguish between hydrogen- and helium-burning red giant stars. *Nature* **471**, 608–611 (2011).
13. Aerts, C., Christensen-Dalsgaard, J. & Kurtz, D. W. Asteroseismology Ch. 3 (Springer-Verlag, 2010).
14. Basu, S. *et al.* Sounding Open Clusters: Asteroseismic Constraints from Kepler on the Properties of NGC 6791 and NGC 6819. *Astrophys. J.* **729**, L10–L15 (2011).
15. Stello, D. *et al.* An Asteroseismic Membership Study of the Red Giants in Three Open Clusters Observed by Kepler: NGC 6791, NGC 6819, and NGC 6811. *Astrophys. J.* **739**, 13–25 (2011).
16. Corsaro, E. *et al.* Asteroseismology of the Open Clusters NGC 6791, NGC 6811, and NGC 6819 from 19 months of Kepler photometry *Astrophys. J.* **757**, 190–202 (2012)
17. Brogaard, K. *et al.* Age and helium content of the open cluster NGC 6791 from multiple eclipsing binary members. II. Age dependencies and new insights. *Astron. Astrophys.* **543**, A106–A122 (2012).
18. Corsaro, E. & De Ridder, J. DIAMONDS: A new Bayesian nested sampling tool. Application to peak bagging of solar-like oscillations. *Astron. Astrophys.* **571**, A71–A92 (2014).
19. Corsaro, E., De Ridder, J., García, R. A. Bayesian peak bagging analysis of 19 low-mass low-luminosity red giants observed with Kepler. *Astron. Astrophys.* **579**, A83–A158 (2015).
20. Meibom, S. *et al.* A spin-down clock for cool stars from observations of the 2.5-billion-year-old cluster. *Nature* **517**, 589–591 (2015).
21. Geller, A. M., Hurley, J. R., & Mathieu, R. D. Direct N-body Modeling of the Old Open Cluster NGC 188: A Detailed Comparison of Theoretical and Observed Binary Star and Blue Straggler Populations. *Astron. J.* **145**, 8–29 (2013).
22. Hut, P. Tidal Evolution in Close Binary Systems. *Astron. Astrophys.* **99**, 126–140 (1981).
23. van den Bergh, S., McClure, R. D. Galactic distribution of the oldest open clusters. *Astron. Astrophys.* **88**, 360–362 (1980).
24. Lee, Y.-N., Hennebelle, P. Formation of a protocluster: A virialized structure from gravoturbulent collapse I. Simulation of cluster formation in a collapsing molecular cloud. *Astron. Astrophys.* **591**, A30–A46 (2016).
25. Platais, I. A. *et al.* A New Look at the Old Star Cluster NGC 6791. *Astrophys. J.* **733**, L1–L5 (2011).
26. Kalirai, J. S. *et al.* The CFHT Open Star Cluster Survey. II. Deep CCD Photometry of the Old Open Star Cluster NGC 6819. *Astron. J.* **122**, 266–282 (2001).
27. Brewer, L. N. *et al.* Determining the Age of the Kepler Open Cluster NGC 6819 With a New Triple System and Other Eclipsing Binary Stars. *Astron. J.* **151**, 66–85 (2016).
28. Miglio, A. *et al.* Asteroseismology of old open clusters with Kepler: direct estimate of the integrated red giant branch mass-loss in NGC 6791 and 6819. *Mon. Not. R. Astron. Soc.* **419**, 2007–2088 (2012).
29. Milliman, K. E. *et al.* WIYN Open Cluster Study. LX. Spectroscopic Binary Orbits in NGC 6819. *Astron. J.* **148**, 38–57 (2014).

Acknowledgements E.C. is funded by the European Community's Seventh Framework Programme (FP7/2007-2013) under grant agreement n°312844 (SPACEINN) and by the European Union's Horizon 2020 research and innovation programme under the Marie Sklodowska-Curie grant agreement n° 664931. Y.-N.L. and P.H. acknowledge funding by the European Research Council under the European Community's Seventh Framework Programme (FP7/2007-2013 grant agreement n° 306483) and the HPC resources of CINES under the allocation x2014047023 made by GENCI (Grand Equipement National de Calcul Intensif). R.A.G. received funding from the CNES GOLF and PLATO grants at CEA. R.A.G. and P.G.B. received funding from the ANR (Agence Nationale de la Recherche, France) program IDEE (n° ANR-12-BS05-0008) "Interaction Des Étoiles et des Exoplanètes". Sa.M. acknowledges support from the NASA grant NNX12AE17G. St.M. acknowledges funding by the European Research Council through ERC grant SPIRE n° 647383. D.S. is the recipient of an Australian Research Council Future Fellowship (project n° FT140100147). J.B. acknowledges financial support from grant ANR 2011 Blanc SIMI5-6 020 "Toupies: Towards understanding the spin

evolution of stars". This work has received funding from the CNES grants at CEA. All the light curves used in this paper were obtained from the Mikulski Archive for Space Telescopes (MAST). STScI is operated by the Association of Universities for Research in Astronomy, Inc., under NASA contract NAS5-26555. Support for MAST for non-HST data is provided by the NASA Office of Space Science via grant NNX09AF08G and by other grants and contracts. UKIRT is supported by NASA and operated under an agreement among the University of Hawaii, the University of Arizona, and Lockheed Martin Advanced Technology Center; operations are enabled through the cooperation of the East Asian Observatory. We thank David Salabert for the preparation of the website containing the source data used in this work.

Author contributions E.C. performed the fits of the background in the power spectra, identified the oscillation modes, measured the mode parameters and the inclination angles for all the stars in the sample, and interpreted the results. Y.-N.L. performed the hydrodynamical simulations of the proto-cluster formation and for the significance of the stellar-spin alignment, and contributed in interpreting the initial conditions in the molecular cloud. R.A.G. prepared the datasets calibrated for the asteroseismic analysis, contributed in discussing the analysis method and the observational results, and reanalyzed the independent sample of stars observed in NGC 6819. P.H. contributed in the computation of the hydrodynamical simulations and in the interpretation of observational results and of the initial conditions in the molecular cloud. Sa.M. provided input guesses for the background properties in the power spectra of all the stars and contributed in the selection of the control sample. P.G.B. contributed in discussing the data analysis method and the identification of the oscillation modes. St.M. contributed in discussing the N-body interactions among stars in open clusters and in quantifying the tidal effects in binary stars. D.S. provided spatial positions for the entire population of red giants identified in the field of the two clusters and contributed in discussing the observational results and the data analysis method. J.B. provided theoretical and observational insights on the effect and evolution of angular momentum in stellar clusters. All authors commented on the manuscript.

Author information Supplementary information is available for this paper. Reprints and permissions information is available at www.nature.com/reprints. Correspondence and requests for materials should be addressed to E.C. (e-mail: enrico.corsaro@oact.inaf.it).

Competing interests The authors declare no competing financial interests.

Open cluster	NGC 6791	NGC 6819
Total mass ($M_\odot$)	~ 5000	~ 2600
Distance modulus $(m-M)_0$	13.11 ± 0.06	11.85 ± 0.05
Size (pc)	~ 10	~ 7
Age (Gyr)	~ 8.3	~ 2.4
Galactic coordinates	70.0 (long.), $+10.9$ (lat.)	74.0 (long.), $+8.5$ (lat.)
$\overline{M}_{\rm RC}$ ($M_\odot$)	1.15 ± 0.03	1.65 ± 0.04
Stars analyzed	25	23

Table 1 | **Global properties of NGC 6791 and NGC 6819.** The total masses in units of a solar mass show that both clusters are massive, with NGC 6791 one of the most massive known in the Galaxy[25,26]. The size is computed in this study by means of the angular radii[25,26] and the distance modulus from asteroseismology[14]. Ages are based on eclipsing binaries and triple systems[17,27]. The galactic coordinates refer to the astronomical epoch J2000. The average mass of a core-He-burning star, $\overline{M}_{\rm RC}$, is calculated from asteroseismic scaling relations and it is comparable to that of the shell-H-burning red giants of the same cluster because of the low mass loss[28]. The total number of stars analyzed refers to the pulsating red giants whose orientation of the spin axis has been measured in this work. The corresponding 1σ random error is shown for distance modulus and average mass of the stars.

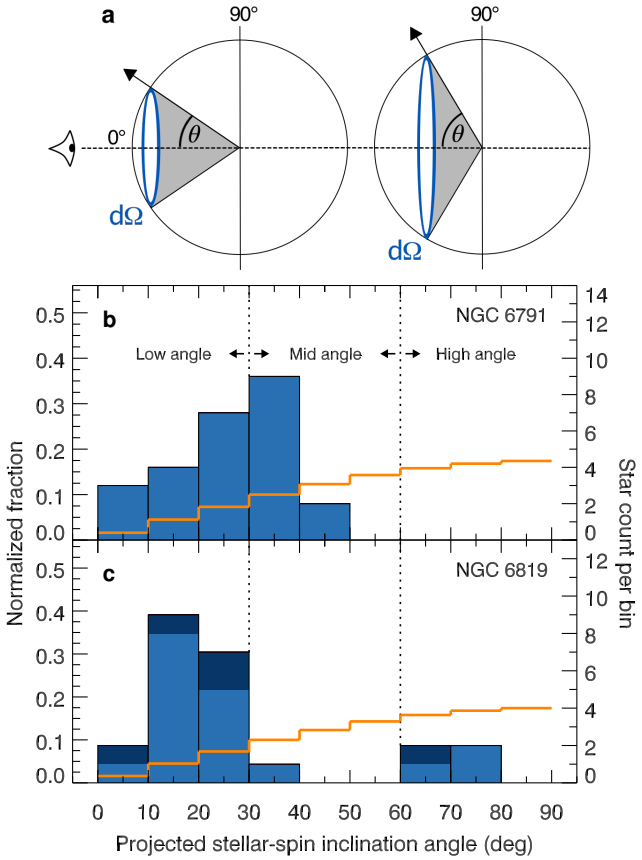

Figure 1 | **Projected stellar-spin inclinations of the 48 red giants of NGC 6791 and NGC 6819. a**, The spin vector of the star (arrow) as seen from the line of sight can be oriented along any directions of a cone (gray shaded), with an inclination angle from $\theta = 0^\circ$ (pole-on) to $\theta = 90^\circ$ (edge-on). The infinitesimal solid angle $d\Omega$ (blue coronal shell) increases by increasing θ. **b**, The distribution of θ from rotationally split $l = 1$ mixed modes for NGC 6791. The orange histogram shows the expected distribution for a three-dimensional uniform orientation of the spin vectors (see Methods). The vertical dotted lines separate the three main configurations of stellar inclination. **c**, Same as panel b but for NGC 6819. The darker regions correspond to red giants that are confirmed spectroscopic single-lined binaries[29].

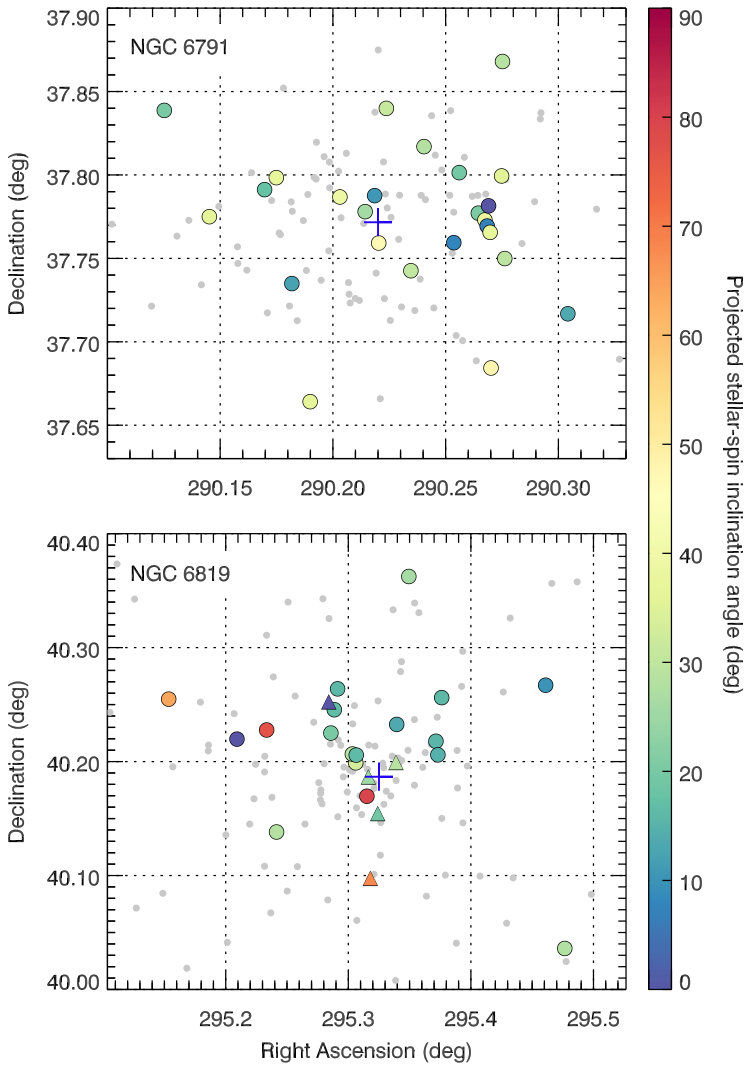

Figure 2 | **Spatial positions of the 48 red giants of NGC 6791 and NGC 6819.** The spatial positions of the red giants analyzed here are shown in spherical coordinates (see Supplementary Tables 1 and 2), with projected inclination angles of the stellar-spin axis indicated by a color-coded scale. The group of four stars at high angles in NGC 6819 appears to be localized along a diagonal in the bottom-left region of the diagram. The spectroscopic binaries of NGC 6819 are indicated by triangles. The entire population of red giants identified in the clusters is shown by the gray dots in the background[15], while the centers of the cluster fields are marked by blue crosses.

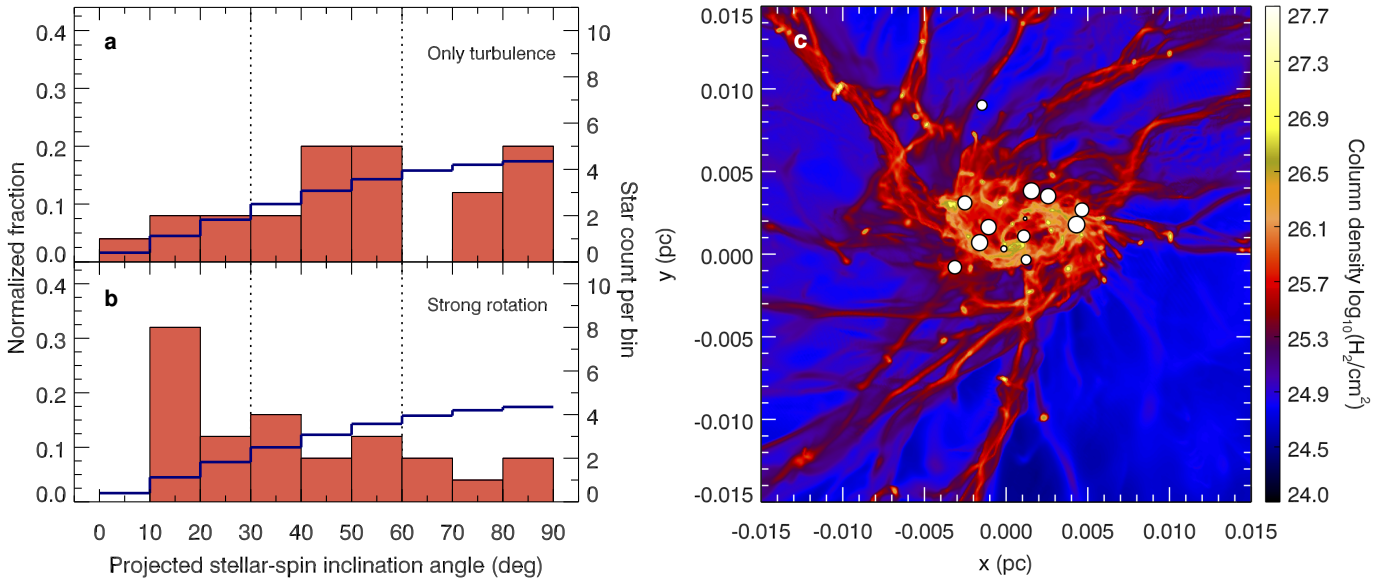

Figure 3 | **Projected stellar-spin inclinations and proto-cluster formation from hydrodynamical simulations. a**, The distribution of θ for 25 stars with $M \geq 0.7\,M_{\odot}$ obtained from the simulation without global rotation (Simulation 1 in Supplementary Table 3), where no stellar-spin alignment is detected. The blue histogram represents the expected three-dimensional uniform distribution. **b**, Same as panel a but for the simulation with the best level of alignment (Simulation 4). **c**, The rotating proto-cluster from Simulation 4 as seen along the axis of best spin alignment $\vec{z}$ (see Methods), with a color-coded column density. White circles represent pre-stellar cores gathering most of the cloud's average angular momentum, with their size proportional to the cosine between their spin axis and $\vec{z}$.

METHODS

Target selection and data preparation. Our red giant stars are selected by having either available estimates of the observed period spacing of mixed dipole modes[16] or asymptotic period spacing of dipole gravity modes, $\Delta\Pi_1$, namely the regular spacing in period that characterizes the gravity modes of oscillation[30,31]. These period spacings ensure us an unambiguous classification of the evolutionary stage of the stars (either shell-H burning or core-He burning) and represent the starting point for a reliable mode identification of the oscillation peaks in the Fourier spectrum. The selected cluster stars have most precise and largest number of identified stellar oscillation frequencies, which makes them the best suited for the measurement of spin inclination. For NGC 6791 we identify 31 stars but we discard KIC 2435987, KIC 2436097, KIC 2436458, KIC 2437240, KIC 2437589 from the analysis because they are red giant branch stars with a low frequency of maximum power ($\nu_{\rm max} \leq 50\,\mu$Hz) and low period spacing ($\Delta\Pi_1 \leq 70$ s). For these stars the identification of the rotational multiplets is not reliable because the frequency separation between adjacent dipole mixed modes is less than 10 times the frequency resolution ($\sim$0.008 μHz, see below). Finally, KIC 2436593 is removed because of the presence of oscillation power excess from two stars. For NGC 6819 we identify 24 stars but we remove KIC 5024967 because few dipolar mixed modes were found.

The Kepler light curves used cover the full observing length (up to quarter 17.2, i.e. 4 years) and were optimized for asteroseismic analysis using an inpainting interpolation[32–34]. We also consider 36 field red giants, obtained by combining already published results for 19 shell-H-burning red giants[19] with a new set of 17 core-He-burning red giants. All these field red giants exhibit a signal-to-noise ratio in the power spectra and masses similar to those of the cluster stars, and were observed by Kepler up to quarter 17.2. These field stars constitute our control sample and are selected using the same criterion as for the cluster red giants, hence through the available period spacings[30,31,35]. The 17 core-He-burning red giants represent all the stars available from the latest release of the Kepler catalogue[36] that satisfy our selection criterion. The large fraction of high spin-inclination angles found for both types of field red giants (see Supplementary Table 5), in agreement with random spin orientation, demonstrates that independently of the evolutionary stage our selection criterion is not introducing any specific bias against high angles.

Background signal, oscillation mode properties, and mode identification. The first step performed in the analysis of the stellar power spectra is the estimation of the background signal (dashed blue line in Supplementary Fig. 1), namely the signal originating from the stellar granulation, the surface rotation, and the instrumental noise. We have adopted the Bayesian code DIAMONDS[18] and a background model defined by three super-Lorentzian profiles (one for the surface rotation and two for the granulation signal), a flat white noise component, and an additional super-Lorentzian profile accounting for the colored noise at low frequency ($< 10\,\mu$Hz), with uniform prior distributions for each free parameter of the background model[19,37]. The prior distributions were set using first guesses obtained by means of the A2Z pipeline[38].

The second step involves the fitting and identification of the individual oscillation modes, a procedure known as peak bagging analysis[18,19]. The fitting is done using DIAMONDS, providing accurate estimates for the properties of mode frequency, linewidth, and amplitude (or height) for each of the oscillation peaks considered. The significance of peaks with a low signal-to-noise ratio (having a height that corresponds to about eight times the background level) is tested by means of Bayesian evidence, and peaks are deemed significant when reaching a detection probability $\geq 99\,\%$. All significant peaks are considered as true oscillation modes and their fitted properties can thus be exploited for further analysis. The mode identification of the acoustic modes ($l = 0, 2, 3$ modes) is done by exploiting the published global asteroseismic parameters of the asymptotic relation for acoustic modes[16,39]. To identify the dipolar mixed modes in our stars we derive accurate

estimates of both $\Delta\Pi_1$ and the coupling factor q of the asymptotic relation of mixed modes[30], using a two-dimensional grid-search method to fit the associated asymptotic relation to the power spectra[19,40]. We use the published values of the observed period spacing or, when available, $\Delta\Pi_1$ as initial guesses for the fits[16,31]. The mode identification process only relies on the value of $\Delta\Pi_1$, and it is performed in exactly the same way for both shell-H-burning and core-He-burning red giants. The asymptotic relation of mixed modes yields the identification of the $m = 0$ components of each mixed mode multiplet. The rotationally split components of dipolar mixed modes, $m = \pm 1$, can then be easily identified thanks to their nearly symmetrical pattern with respect to the central non-split component, $m = 0$. An example result of the complete analysis process for one cluster red giant is provided in Supplementary Fig. 1. The same approach is applied to the control sample.

Extraction of projected stellar-spin inclination. The fitting of the projected inclination of the stellar-spin axis is done subsequently to the peak bagging analysis. For this purpose, we first select from four to seven different rotationally-split multiplets of $l = 1$ mixed modes identified from the power spectra of each star. Each multiplet can be described by one to three oscillation peaks (m components), which are fit independently from one another during the peak bagging analysis to allow for a better match to the observations. The multiplets are chosen in a way that they cover at least two different but consecutive radial mode orders. The radial mode orders considered are those containing the highest signal-to-noise ratio peaks, hence the closest to $\nu_{\max}$. By choosing the highest signal-to-noise peaks we guarantee a better and more reliable constraint of the inclination angle during the fitting process. In addition, the selected multiplets are in the most p-dominated regions of the mixed mode forest, which provides a closer resemblance to the concept of energy equipartition and therefore of the visibility within the m components of the multiplet[6]. Once the multiplets are chosen, we consider only those m components that correspond to peaks deemed significant during the peak bagging analysis. This prevents us, independently of the signal-to-noise ratio in the power spectra, from using peaks that could constitute just pure noise, otherwise hampering the reliability of the results.

The oscillation mode properties of frequency, linewidth and amplitude (or height) of each m component of a multiplet are used to build its 3-component fitting model profile[6,10,11], constructed as the sum of the same peak-profile functions used during the peak bagging analysis. The model profile is constrained by setting its total power density to the value given by the sum of the heights of its individual m components, as measured by the peak bagging analysis. The frequency of each multiplet component m is set to the already available frequency value extracted with the peak bagging analysis. When the central component ($m = 0$) is missing (or not detected), we use the average frequency of the $m = \pm 1$ components as central frequency. When one of the two side components ($m = \pm 1$) is missing (or not detected), we use the symmetric value with respect to that of $m = 0$ as its frequency. When the two side components (both $m = +1$ and $m = -1$) are missing (or not detected) the stellar spin inclination angle must be very low. In this latter case the choice of the frequencies of the split components does not typically influence the fit. However, we approximate these frequencies using a reasonable value of the average rotational splitting $\overline{\delta\nu}_{\rm rot}$, as obtained from the complete set of peak-bagged dipolar mixed modes of the star (see Supplementary Tables 1 and 2 for all the values of $\overline{\delta\nu}_{\rm rot}$).

Finally, we perform the fits using a Bayesian parameter estimation of the inclination angle θ, which represents the free parameter of the 3-component model profile previously defined. By varying the inclination angle, the relative heights of the three m components change by redistributing the total power of the multiplet among its different peaks. When the inclination angle is high ($\theta \sim 90^\circ$), the central component contains most of the power, while for low inclination angles ($\theta \sim 0^\circ$) the central component disappears because the power is equally distributed to the two side components, which exhibit both the same height. For the parameter estimation we use a uniform

prior on $\cos\theta$ for $5^\circ < \theta < 85^\circ$ and a uniform prior on θ for $0^\circ \leq \theta \leq 5^\circ$ and $85^\circ \leq \theta \leq 90^\circ$, and an exponential likelihood function, as adopted for the fitting of the power spectra[18]. The multiplets are fit all together at the same time, for providing a more robust and better constrained estimate of θ. An example of the resulting fit to θ for one red giant star of our sample is shown in Supplementary Fig. 1, while the inclination angles are given in Supplementary Tables 1 and 2. The same fitting technique is applied to the control sample, and the results are listed in Supplementary Table 5.

Simulation of three-dimensional distribution of uniform stellar-spin orientation. When observing a sample of stars with a uniform orientation of their stellar-spin vectors in a three-dimensional space, the geometrical effect from the line of sight shown in Fig. 1a, introduces an observational bias toward high inclination angles. This is happening because the number of stars per projected inclination angle is proportional to the associated solid angle, which follows the law $d\Omega = \sin\theta d\theta$. Therefore, to obtain a realistic distribution of a uniform orientation of the spin vector in three dimensions we simulate a uniform (flat) distribution in $-1 \leq \cos\theta \leq 1$, and subsequently fold it into $0 \leq \cos\theta \leq 1$ to account for the degeneracy between θ and $(\theta - \pi)$ arising from the symmetry of the problem. This yields the theoretical histogram shown overlaid in Fig. 1b, c, and 3a, b.

Probability of finding two clusters with strong stellar-spin alignment distributions. We first describe the distributions of spin inclinations shown in Fig. 1b, c using a Gaussian having the mean stellar-spin inclination angle for a cluster as a centroid $\overline{\theta}$, and a standard deviation σ_θ reflecting the sample dispersion around the mean. This yields an interval in inclination angle for each cluster defined as $\left[\overline{\theta} - \sigma_\theta, \overline{\theta} + \sigma_\theta\right]$. The intervals are $[14^\circ, 39^\circ]$ and $[6^\circ, 51^\circ]$ for NGC 6791 and NGC 6819, respectively. Then we consider a random distribution of spin-inclinations as described in the previous paragraph, and derive the cumulative probability of measuring an inclination angle in the range $[\theta_1, \theta_2]$, with $\theta_1 < \theta_2$, to be $p = \int_{\theta_1}^{\theta_2} d\Omega$, which using the definition of solid angle described in the previous paragraph results in $p = \cos\theta_1 - \cos\theta_2$. For the inclination intervals defined by our distributions we obtain that $p_{\rm NGC\ 6791} \simeq 20\,\%$, and $p_{\rm NGC\ 6819} \simeq 36\,\%$, which yields the joint probability of $\sim 7.2\%$ to find two clusters with the observed distributions of stellar-spin inclinations. While this value is low, one needs to realize that strong alignment is a more likely conclusion if the inclination angle is small. This is because a spin-inclination distribution of a strong alignment that peaks at low angles, stands out more significantly relative to the expected distribution from a uniform orientation, which instead has its maximum at $\theta = 90^\circ$ (see Fig. 1b, c, and 3a, b).

Three-dimensional hydrodynamical simulations of proto-cluster formation. The simulations of cluster formation are performed with RAMSES[41,42], a magnetohydrodynamic (MHD) code with adaptive mesh refinement. We simulate the self-gravitating collapse of a molecular cloud following ideal MHD equations. We initialize the simulations with a Bonnor-Ebert-like spherical molecular cloud[24] of $10^3 M_\odot$ and density

$$\rho(r) = \rho_0 \left[1 + \left(\frac{r}{r_0}\right)^2\right]^{-1} .$$

A polytropic equation of state is used such that the gas is isothermal 10 K at low density and heats up adiabatically as $T \propto \rho^{2/3}$ at a turn-over density of 10^{10} $H_2\,cm^{-3}$. The molecular cloud is seeded with an initial turbulent velocity field, solid body global rotation, and no magnetic field. We investigate initial conditions with different levels of turbulence and rotation. We list the parameters in Supplementary Table 3.

The initial molecular cloud is set to be very compact and dense such that a mass of $10^3\,M_\odot$ is contained in a sphere having a diameter of 0.17 pc. This choice was made due to the compromise between obtaining sufficient statistics — for achieving a number of forming stars comparable to that from the observations — and resolving the dynamics of the cloud at stellar scales[24], namely a

few astronomical units. Despite the initial size, the cluster expands after gas expulsion due to the shallowing of the gravitational potential.

To study the stars formed inside the molecular cloud, sink particle algorithms are used[24]. Once the density reaches the threshold of $10^{10}\,\mathrm{H_2\,cm^{-3}}$, we detect the mass concentration and check whether the mass is virially unstable and the flow is locally converging. Subsequently, sink particles are used to follow the Lagrangian mass. The momentum and the angular momentum of the accreted material is added to the sink. We then consider the stars having accreted more than 0.7 $M_\odot$ and examine their spin axis. Varying the mass threshold toward higher values has no impact on the significance of the alignment level. This mass threshold is thus a reasonable value above which stars begin to show a significant spin alignment.

With simulations, we have access to the three-dimensional information and we can choose to project the quantities in any selected orientation. We show that certain initial conditions result in a stellar cluster that has a preferred orientation of rotation. The choice of the projection vector $\vec{z}$ is as follows: we have the matrix $\mathbf{J}$ of which each of the N rows is the unit vector $\vec{j}_i$ of a single star's spin axis, where N is the number of stars considered. To find the maximal alignment, we maximize the quantity

$$\sum_{i=1}^{N}\left(\vec{j}_i\cdot\vec{z}\right)^2=\vec{z}^{\,T}\mathbf{J}^T\mathbf{J}\;\vec{z}\,.$$

The vector that gives us the best observed alignment is the eigenvector corresponding to the largest eigenvalue α of the matrix $\mathbf{J}^T\mathbf{J}/N$. If the orientation is uniform in three-dimensions, we expect this matrix to have three equal eigenvalues at $1/3$.

Spin-alignment level and its significance. The alignment coefficient of a sample of N stars is

$$\alpha=\frac{1}{N}\sum_{i=1}^{N}\cos^2\theta_i\,.$$

For a perfect alignment along the line of sight $\alpha=1$, while for $\alpha=1/3$ the distribution of projected spin inclinations coincides with the ideal uniform distribution in three dimensions, obtained for $N\to\infty$. In the real case with a finite number of stars, the associated uniform distribution can show an intrinsic alignment ($\alpha>1/3$). To quantify its significance according to the number of stars in our sample we have performed five sets of 10000 simulations of three-dimensional uniform stellar-spin orientation, hence we computed the alignment coefficient for each set. The resulting values of α are listed in Supplementary Table 4, and they decrease with increasing number of stars. Using the statistical test of the p-value with the null hypothesis of having a three-dimensional uniform orientation of spin axes, these simulations show that for Simulation 1 (Supplementary Table 3) there is no alignment, for Simulations 2 and 3 only a marginal alignment (about 1σ), and for Simulation 4, representing the case with the strongest rotational energy contribution, we have a significant alignment (over 3σ). The observed distributions for NGC 6791 and NGC 6819 are largely significant (over 6 and 5σ, respectively). However, for the independent control sample of 36 stars, the alignment coefficient is in agreement (within 1σ) with the expected value for spin axes randomly distributed in three dimensions. The agreement (within 1σ) with a random distribution is found even by considering subsamples of field stars having the same evolutionary stage.

Comparison with an independent sample of stars in NGC 6819. A sample of 30 main-sequence stars observed by Kepler and belonging to NGC 6819 has measurements of rotational periods ($P_{\rm rot}$), with a subsample of 25 stars having also projected equatorial velocities ($v\sin\theta$) available[20]. Among the 10 stars having $P_{\rm rot}<17$ days (hereafter fast rotating stars), the five stars in the range $5<v\sin\theta<15$ km s^{-1} are cluster members that hint at high spin-inclination angles because they

match $P_{\rm rot}$–$v \sin\theta$ tracks at constant stellar radius and $\theta = 90^{\circ}$. These stars may not appear compatible with the average low spin-inclination angle found for NGC 6819 in this work. However our reanalysis of the rotational periods for the entire sample of 30 stars reveals that, while confirming most of the published measurements for stars having $P_{\rm rot} > 17$ days, we cannot confirm the periods for the 10 fast rotating stars. We note that this has no implications on the gyrochronology results of NGC 6819 since all these fast rotating stars are the most massive of the sample and were not used for estimating the cluster age[20].

The published rotation periods for the fast rotating stars were obtained using light curves produced by a version of the NASA Kepler data processing pipeline known to affect the stellar signal with periods longer than 3 days due to high-pass filtering[43]; thus potentially biasing stars with slow rotation toward a false fast rotation. Hence for our measurements of rotation periods we instead use a different methodology to prepare light curves[32,44–46] that has been shown to be robust also for slow rotators[47].

Among the 10 fast rotating stars we find reliable periods for only four stars (KIC 5111834, KIC 5023899, KIC 5023760, KIC 5113601). Their periods range from 25 to about 40 days, hence significantly longer than those already published. For these stars the amplitude of the modulation is small (~ 1000 parts-per-million magnitude). This could arise either because of star spots seen from a low spin-inclination angle, or blending with fainter cool active main-sequence stars. We conclude that for these stars further observations are required to confirm their published $v \sin\theta$ (available only for KIC 5111834 and KIC 5113601), and therefore to be able to disentangle the two mentioned effects. For the remaining six fast rotating stars we find that two stars (KIC 5024227 and KIC 5026583, with the latter having $v \sin\theta$ available) do show an ambiguous rotation period in our analysis and that four stars (KIC 4938993, KIC 5024122, KIC 5111207, KIC 5112499, with the first two having $v \sin\theta$ measurements) could be polluted by nearby stars seen in United Kingdom Infra-Red Telescope (UKIRT) high-resolution images. In the latter four cases, one or two additional stars are located within a four-Kepler-pixel square around the target, preventing us from being certain of which star is actually responsible for the alleged rotational signal found in the Kepler photometry. We therefore caution the use of these six stars when drawing conclusions about the general rotational properties of the cluster. The comparison is shown in Supplementary Fig. 2 and 3. In conclusion, about 70% of the main-sequence cluster stars having both published $v \sin\theta$ and reliable period detections from our analysis, are compatible with a low spin-inclination regime, therefore in agreement with the findings presented in this work.

Data availability. The datasets analyzed and the results generated during the current study are available in the CEA Saclay repository,
http://irfu.cea.fr/Phocea/Vie_des_labos/Ast/ast_technique.php?id_ast=3801. The original raw Kepler light curves were obtained from the MAST, available at https://archive.stsci.edu/index.html. The power spectra were obtained using the commercially available IDL routine *lnp_test*. The inpainting interpolation software K-Inpainting is publicly available at
http://irfu.cea.fr/Sap/en/Phocea/Vie_des_labos/Ast/ast_visu.php?id_ast=3346. The Bayesian inference code DIAMONDS is publicly available and documented at
https://fys.kuleuven.be/ster/Software/Diamonds/. The simulation of the three-dimensional uniform orientation of the spin vectors and the Bayesian fits to the projected inclination angles are obtained using built-in IDL routines and subroutines, which are therefore not made publicly available. The RAMSES code package for the three-dimensional hydrodynamical simulations is publicly available and documented at https://bitbucket.org/rteyssie/ramses/wiki/.

30. Mosser, B. *et al.* Probing the core structure and evolution of red giants using gravity-dominated mixed modes observed with Kepler. *Astron. Astrophys.* **540**, A143–A153 (2012).

31. Mosser, B. *et al.* Mixed modes in red giants: a window on stellar evolution. *Astron. Astrophys.* **572**, L5–L9 (2014).
32. García, R. A. *et al.* Preparation of Kepler light curves for asteroseismic analyses. *Mon. Not. R. Astron. Soc.* **414** L6–L10 (2011).
33. García, R. A. *et al.* Impact on asteroseismic analyses of regular gaps in Kepler data. *Astron. Astrophys.* **568**, A10–A18 (2014).
34. Pires, S. *et al.* Gap interpolation by inpainting methods: Application to ground and space-based asteroseismic data. *Astron. Astrophys.* **574**, A18–A27 (2014).
35. Vrard, M., Mosser, B., Samadi, R. Period spacings in red giants. II. Automated measurement. *Astron. Astrophys.* **588**, 87–99 (2016).
36. Mathur, S. *et al.* Revised Stellar Properties of Kepler Targets for the Q1-17 (DR25) Transit Detection Run. Preprint at https://arxiv.org/abs/1609.04128 (2016).
37. Kallinger, T. *et al.* The connection between stellar granulation and oscillation as seen by the Kepler mission. *Astron. Astrophys.* **570**, A41–A57 (2014).
38. Mathur, S. *et al.* Determining global parameters of the oscillations of solar-like stars. *Astron. Astrophys.* **511**, A46–A58 (2010).
39. Tassoul, M. Asymptotic approximations for stellar nonradial pulsations. *Astrophys. J. Suppl. Ser.* **43**, 469–490 (1980).
40. Buysschaert, B. *et al.* Testing the asymptotic relation for period spacings from mixed modes of red giants observed with the Kepler mission. *Astron. Astrophys.* **588**, A82–A95 (2016).
41. Teyssier, R. Cosmological hydrodynamics with adaptive mesh refinement. A new high resolution code called RAMSES. *Astron. Astrophys.* **385**, 337–364 (2002).
42. Fromang, S., Hennebelle, P., Teyssier, R. A high order Godunov scheme with constrained transport and adaptive mesh refinement for astrophysical magnetohydrodynamics. *Astron. Astrophys.* **457**, 371–384 (2006).
43. Garcia, R. A. *et al.* Measuring Reliable Surface Rotation Rates from Kepler Photometric Observations. *Astron. Soc. Pac.* **479**, 129–136 (2013).
44. McQuillan, A., Mazeh, T., Aigrain, S. Rotation Periods of 34,030 Kepler Main-sequence Stars: The Full Autocorrelation Sample. *Astrophys. J. Suppl. Ser.* **211**, 24–37 (2014).
45. García, R. A. *et al.* Rotation and magnetism of Kepler pulsating solar-like stars. Towards asteroseismically calibrated age-rotation relations. *Astron. Astrophys.* **572**, 34–48 (2014).
46. Ceillier, T. *et al.* Rotation periods and seismic ages of KOIs - comparison with stars without detected planets from Kepler observations. *Mon. Not. R. Astron. Soc.* **456**, 119–125 (2016).
47. Aigrain, S. *et al.* Testing the recovery of stellar rotation signals from Kepler light curves using a blind hare-and-hounds exercise. *Mon. Not. R. Astron. Soc.* **450**, 3211–3226 (2015).

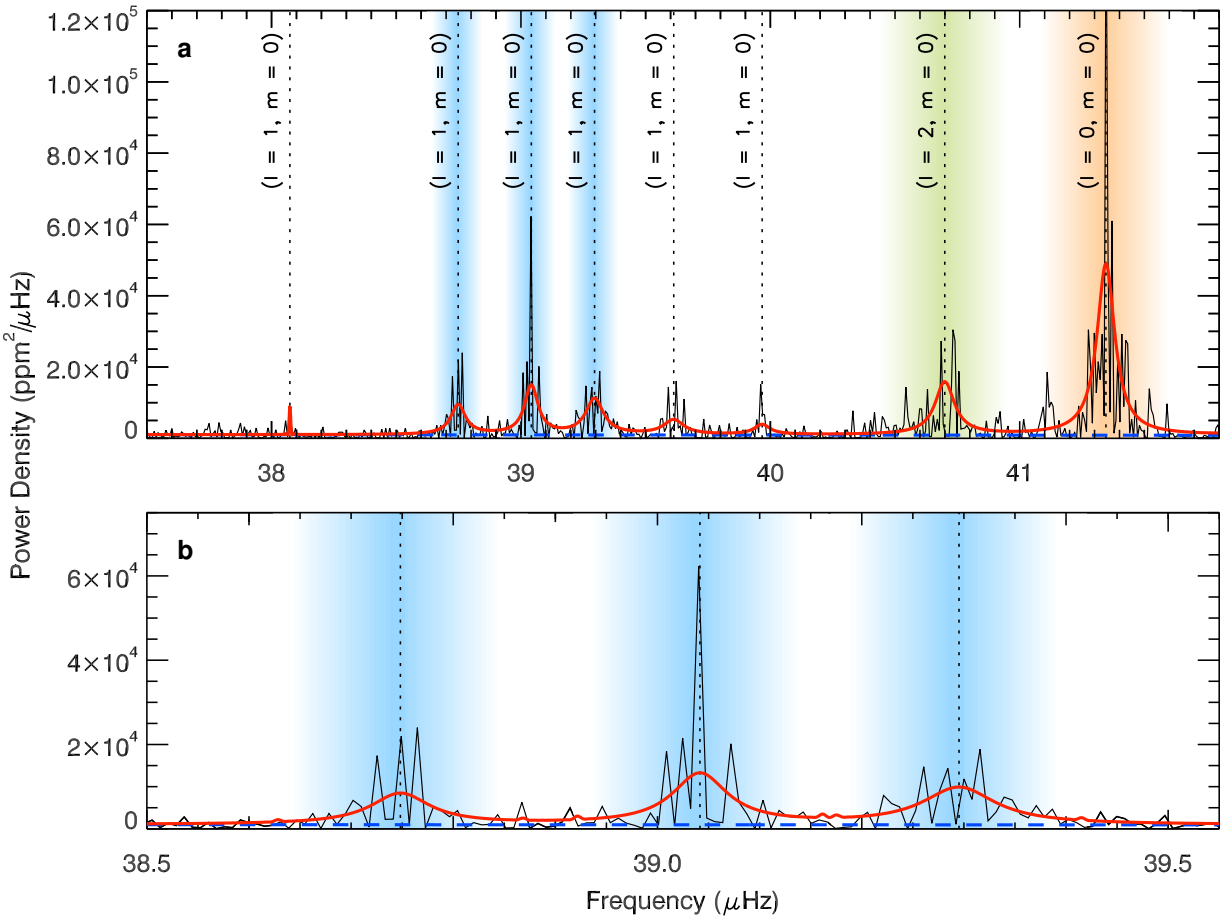

Supplementary Figure 1 | **Bayesian peak bagging analysis and fit to the inclination angle. a**, A chunk of power spectrum for the core-He-burning red giant KIC 5112373 having a low inclination angle. The Bayesian fit to the oscillations[18,19] is indicated by the red line, with the individual mode frequencies marked by a vertical dotted line and the mode identification by labels. The green and orange vertical bands highlight the regions containing the quadrupole ($l = 2$) and radial ($l = 0$) modes, respectively. The blue bands indicate the three dipolar mixed modes used to fit the inclination angle of the stellar spin (see Methods). The dashed blue line shows the level of the background signal. **b**, A close-up in the region containing the three dipolar mixed modes marked by a blue vertical band, with the red line here showing the resulting Bayesian fit to the inclination angle.

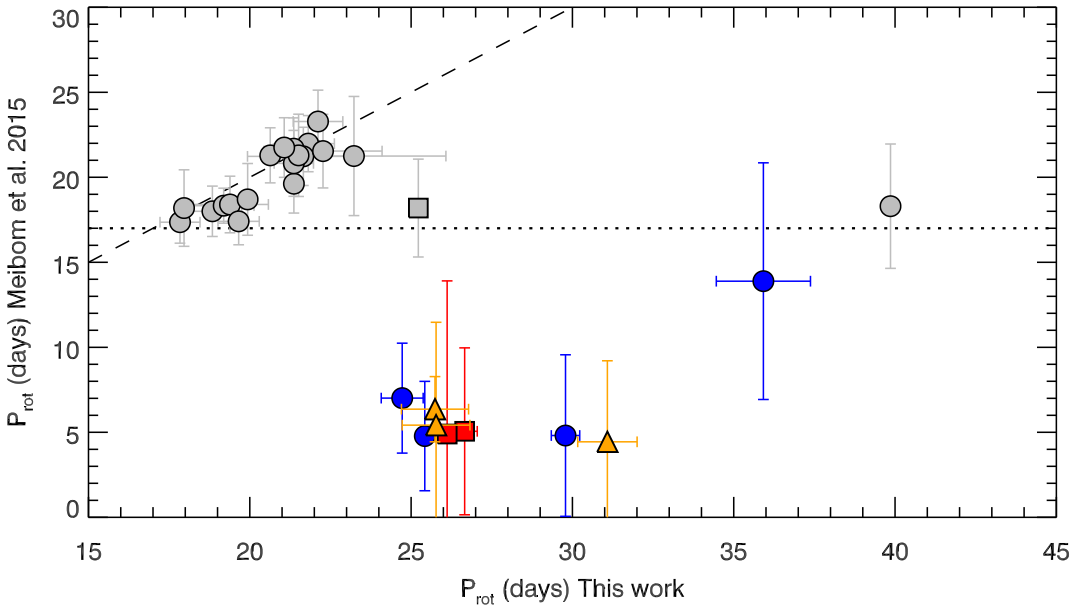

Supplementary Figure 2 | **Comparison of new rotation periods with published values for 30 stars in NGC 6819.** The published rotational periods[20] are compared with the results from our new reanalysis of the same targets (see Methods for more details). Colored symbols correspond to stars discussed in the text (blue circles for clear detection, red squares for unreliable detection, orange triangles for polluted). KIC 4938993, one of the polluted targets, is not displayed because no period measurement could be obtained for this star. The dashed line corresponds to a one-to-one match while the dotted line delimits the threshold of the fast rotating stars selected in this work, $P_{\rm rot} = 17$ days. All symbols shown in gray correspond to stars with $P_{\rm rot} > 17$ days (circles for clear detections and a square for KIC 5024856, the only slow rotating star with unreliable detection).

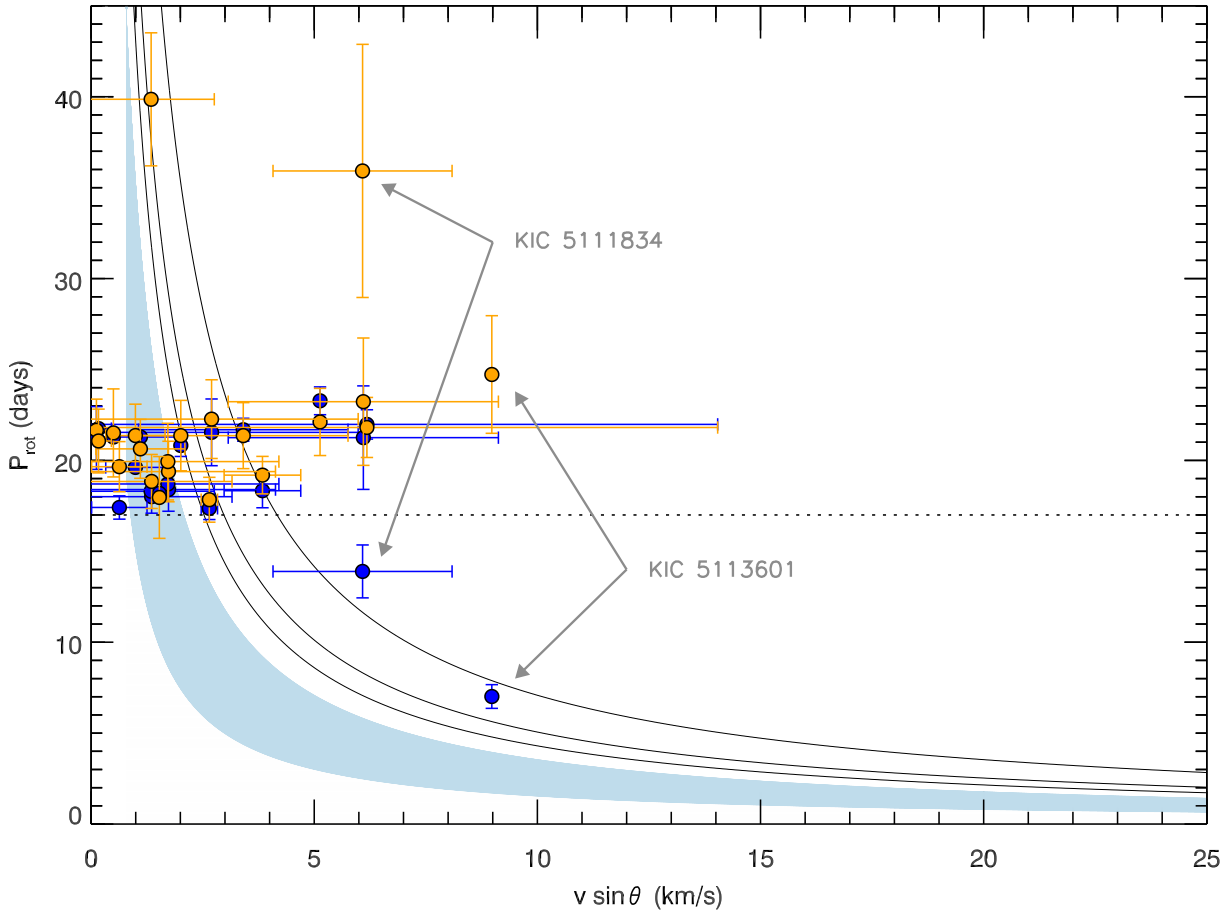

Supplementary Figure 3 | **Rotation periods versus published projected equatorial velocities for 21 stars in NGC 6819**. The published rotational periods[20] (blue circles) are compared to those from our analysis (orange circles) for the stars found to have reliable period detections (see Methods). The published $v \sin\theta$ measurements[20] are kept the same for both sets of period measurements. The horizontal dotted line delimits the threshold of the fast rotating stars discussed here, $P_{\rm rot} = 17$ days. The only two fast rotating stars with reliable period detection from our analysis are indicated by arrows, with KIC IDs overlaid. Tracks at constant radii ($R = 0.85, 1.0, 1.4\,R_{\odot}$) and inclination angle $\theta = 90°$ are shown. The shaded region delimits a regime of low spin inclination ($\theta = 20$-$30°$) and stellar radius $0.85\,R_{\odot} \leq R \leq 1.4\,R_{\odot}$.

KIC ID	Right Ascension (deg)	Declination (deg)	θ (deg)	$\overline{\delta\nu}_{\rm rot}$ (μHz)	Evolutionary stage
2297384	290.1899	37.6641	36^{+3}_{-3}	0.055	RC
2297825	290.2701	37.6843	48^{+4}_{-4}	0.050	RC
2436417	290.1452	37.7750	37^{+3}_{-3}	0.063	RC
2436676	290.1697	37.7912	18^{+6}_{-6}	0.250	RGB
2436732	290.1749	37.7984	37^{+3}_{-3}	0.072	RC
2436818	290.1818	37.7349	13^{+6}_{-5}	0.180	RGB
2437103	290.2031	37.7868	39^{+4}_{-4}	0.121	RC
2437270	290.2143	37.7780	26^{+5}_{-4}	0.122	RGB
2437325	290.2185	37.7876	11^{+5}_{-5}	0.150	RGB
2437353	290.2203	37.7592	47^{+3}_{-3}	0.066	RC
2437564	290.2346	37.7426	30^{+3}_{-3}	0.070	RC
2437804	290.2536	37.7594	8^{+5}_{-5}	0.050	RC
2437933	290.2645	37.7771	20^{+5}_{-5}	0.200	RGB
2437957	290.2674	37.7730	38^{+3}_{-3}	0.184	RGB
2437972	290.2684	37.7694	8^{+4}_{-4}	0.150	RGB
2437976	290.2690	37.7815	0^{+10}_{-10}	0.180	RGB
2437987	290.2697	37.7656	38^{+3}_{-3}	0.057	RC
2438038	290.2748	37.7994	36^{+3}_{-3}	0.045	RGB
2438051	290.2762	37.7499	30^{+4}_{-4}	0.062	RC
2438333	290.3042	37.7168	14^{+3}_{-3}	0.080	RGB
2569055	290.1252	37.8387	20^{+6}_{-5}	0.120	RC
2569945	290.2237	37.8399	31^{+3}_{-3}	0.083	RC
2570094	290.2404	37.8170	28^{+3}_{-3}	0.066	RGB
2570244	290.2560	37.8014	20^{+3}_{-3}	0.172	RGB
2570384	290.2752	37.8680	29^{+4}_{-4}	0.040	RGB

Supplementary Table 1 | **Positions and stellar-spin inclinations for the red giants of NGC 6791.** All the declinations and right ascensions refer to the astronomical epoch J2000. The inclination angles are the median values, with corresponding 68.3 % credible intervals, obtained from a Bayesian parameter estimation (see Methods). The average rotational splitting, $\overline{\delta\nu}_{\rm rot}$, is a reference value per star. The evolutionary stage distinguishes between core-He-burning (RC) and shell-H-burning red giants (RGB), and it is derived from the available period spacings used for the peak bagging analysis[16,30,31].

KIC ID	Right Ascension (deg)	Declination (deg)	θ (deg)	$\overline{\delta\nu_{\rm rot}}$ (μHz)	Evolutionary stage
4937056*	295.3180	40.0975	68^{+5}_{-5}	0.084	RC
4937770	295.4766	40.0360	28^{+3}_{-3}	0.265	RC
5023953	295.2415	40.1382	29^{+4}_{-4}	0.204	RC
5024327	295.3061	40.1989	33^{+3}_{-3}	0.112	RC
5024404	295.3152	40.1696	80^{+10}_{-4}	0.125	RC
5024414*	295.3164	40.1865	26^{+5}_{-4}	0.351	RC
5024476*	295.3240	40.1544	20^{+7}_{-6}	0.180	RC
5024582*	295.3389	40.1992	29^{+4}_{-4}	0.141	RC
5111718	295.1535	40.2548	64^{+4}_{-4}	0.249	RGB
5111949	295.2092	40.2197	0^{+11}_{-11}	0.200	RC
5112072	295.2334	40.2277	77^{+6}_{-7}	0.220	RGB
5112361*	295.2841	40.2524	0^{+7}_{-7}	0.150	RGB
5112373	295.2858	40.2250	20^{+8}_{-6}	0.120	RC
5112387	295.2886	40.2455	17^{+8}_{-7}	0.150	RC
5112401	295.2913	40.2638	16^{+9}_{-8}	0.080	RC
5112467	295.3033	40.2066	28^{+6}_{-4}	0.137	RC
5112491	295.3065	40.2057	17^{+8}_{-8}	0.150	RC
5112730	295.3395	40.2326	14^{+8}_{-8}	0.120	RC
5112938	295.3715	40.2178	16^{+9}_{-8}	0.120	RC
5112950	295.3731	40.2059	15^{+8}_{-7}	0.170	RC
5112974	295.3762	40.2561	16^{+8}_{-6}	0.150	RC
5113441	295.4610	40.2670	10^{+5}_{-9}	0.500	RGB
5200152	295.3494	40.3624	26^{+6}_{-5}	0.149	RC

Supplementary Table 2 | **Positions and stellar-spin inclinations for the red giants of NGC 6819.** All the declinations and right ascensions refer to the astronomical epoch J2000. The inclination angles are the median values, with corresponding 68.3 % credible intervals, obtained from a Bayesian parameter estimation (see Methods). The average rotational splitting, $\overline{\delta\nu_{\rm rot}}$, is a reference value per star. The evolutionary stage distinguishes between core-He-burning (RC) and shell-H-burning red giants (RGB), and it is derived from the available period spacings used for the peak bagging analysis[16,30,31]. The stars marked with an asterisk are the spectroscopic single-lined binaries[29] indicated in Fig. 1 and 2.

Simulation #	$E_{\rm ther}/E_{\rm grav}$	$E_{\rm tur}/E_{\rm grav}$	$E_{\rm rot}/E_{\rm grav}$	α
1	0.0025	1.51	0	0.40
2	0.0025	1.12	0.15	0.48
3	0.0025	0.46	0.15	0.45
4	0.0025	0.15	0.15	0.59

Supplementary Table 3 | **Energy balancing and alignment parameters of the simulations.** The simulated molecular cloud has a mass of $10^3\,M_\odot$ and a radius of $0.084\,$pc. The various forms of energy used for the different simulations are reported in relative values for the portion of molecular cloud forming the protocluster (containing about $140\,M_\odot$). The thermal energy $E_{\rm ther}$, turbulent kinetic energy $E_{\rm tur}$, and rotational kinetic energy $E_{\rm rot}$, counteract the gravitational potential energy $E_{\rm grav}$ and provide global support for the collapsing cloud. The alignment coefficient α is computed according to its definition (see Methods). All the simulations were run until 25 stars with $M \geq 0.7\,M_\odot$ are formed.

N	α	Skewness
17	0.415 ± 0.071	2.187
19	0.410 ± 0.068	2.165
23	0.402 ± 0.062	2.278
25	0.400 ± 0.060	2.374
36	0.390 ± 0.047	2.005

Supplementary Table 4 | **Alignment coefficients from simulations of uniform stellar-spin inclination.** The most likely alignment coefficient α and its 1σ uncertainty are computed from a skewed Gaussian probability distribution. The distributions are each obtained from 10000 simulations of random stellar-spin orientation in three dimensions. Each distribution corresponds to a different number of stars, N. The adopted numbers of stars are chosen according to those from the observations.

KIC ID	θ (deg)	$\overline{\delta\nu_{\rm rot}}$ (μHz)	Evolutionary stage
3662421	83^{+2}_{-2}	0.163	RC
3744043	37^{+3}_{-3}	0.182	RGB
3954857	86^{+4}_{-2}	0.149	RC
3965149	42^{+6}_{-6}	0.096	RC
4253026	75^{+2}_{-2}	0.108	RC
5709182	38^{+3}_{-3}	0.084	RC
6117517	18^{+3}_{-3}	0.274	RGB
6144777	61^{+2}_{-2}	0.177	RGB
6363338	90^{+4}_{-4}	0.170	RC
6535641	24^{+5}_{-5}	0.040	RC
6604616	90^{+4}_{-4}	0.093	RC
6936990	72^{+3}_{-3}	0.058	RC
7025568	42^{+2}_{-2}	0.149	RC
7060732	79^{+1}_{-1}	0.225	RGB
7619745	90^{+8}_{-8}	0.228	RGB
8366239	74^{+3}_{-3}	0.149	RGB
8475025	90^{+3}_{-3}	0.229	RGB
8547122	83^{+5}_{-4}	0.091	RC
8718745	23^{+2}_{-2}	0.287	RGB
9145955	10^{+6}_{-6}	0.180	RGB
9267654	90^{+3}_{-3}	0.312	RGB
9412305	58^{+5}_{-5}	0.081	RC
9475697	32^{+3}_{-3}	0.222	RGB
9779708	38^{+3}_{-3}	0.045	RC
9882316	0^{+6}_{-6}	0.400	RGB
9907009	46^{+4}_{-4}	0.058	RC
10014635	30^{+3}_{-4}	0.082	RC
10123207	0^{+3}_{-3}	0.400	RGB
10200377	0^{+3}_{-3}	0.300	RGB
10257278	84^{+4}_{-3}	0.332	RGB
11200291	28^{+3}_{-3}	0.042	RC
11353313	72^{+2}_{-2}	0.346	RGB
11570459	54^{+3}_{-3}	0.052	RC
11913545	90^{+5}_{-5}	0.196	RGB
11968334	56^{+2}_{-2}	0.283	RGB
12008916	90^{+5}_{-5}	0.299	RGB

Supplementary Table 5 | **Stellar-spin inclinations for the control sample of field red giants.** The control sample includes the 19 shell-H-burning red giants with detailed peak bagging parameters already available[19], and additional 17 core-He-burning red giants[36]. All the inclination angles were measured using the same approach as for the cluster stars. The inclination angles are the median values, with corresponding 68.3 % credible intervals, obtained from a Bayesian parameter estimation (see Methods). The evolutionary stage is obtained from published period spacings[19,31,35]. The average rotational splitting, $\overline{\delta\nu_{\rm rot}}$, is a reference value per star.